



# Fracture Properties of Waste Marble Powder-slag-based Alkali-Activated Concrete

Xiaofang Deng<sup>1,2</sup>, Dongdong Li<sup>1,2</sup>, Yuwen Chen<sup>1,2</sup>, Ling Lu<sup>1,2</sup> and Bing Liu<sup>1,2\*</sup>

<sup>1</sup> Guangxi Key Laboratory of Green Building Materials and Construction Industrialization, Guilin University of Technology, Guilin, China, 541004

<sup>2</sup> School of Civil Engineering, Guilin University of Technology, Guilin, China, 541004  
cnulb@glut.edu.cn

**Abstract.** Alkali-activated concrete is a new type of environmentally friendly building material. The use of industrial waste marble powder to prepare alkali-activated concrete can reduce energy consumption. This study investigates the fracture properties of waste marble powder-slag-based alkali-activated concrete (WSAAC) by varying the modulus of alkali activators, sodium oxide content, and slag content through three-point bending tests, while analyzing crack development paths using DIC technology. The initial fracture toughness and unstable fracture toughness of WSAAC are positively correlated with its compressive strength. The fracture energy of WSAAC increases initially and then decreases with an increase in the modulus of alkali activators. Moreover, the fracture energy exhibits a gradual increase with higher sodium oxide and slag content.

**Keywords:** Fracture toughness, Fracture energy, Alkali-activated concrete, Waste marble powder.

## 1 Introduction

Concrete is among the most extensively utilized construction materials globally. The CO<sub>2</sub> emissions from ordinary Portland cement production account for about 5 % to 7 % of global CO<sub>2</sub> emissions [1], which is one of the important reasons for the greenhouse effect. Therefore, it is urgent to find a new environmentally friendly material as a replacement for ordinary Portland cement. Many scholars have carried out a series of research and have found that alkali-activated cementitious material is a new material that can replace ordinary Portland cement [2,3]. Alkali-activated concrete offers excellent mechanical properties, high early strength, fire resistance, and durability [4]. Most studies indicate that waste marble powder can serve as a viable substitute for cement [5], a mineral substitute [6], or an inert material [7] in concrete. The research on utilizing waste marble powder as a precursor for alkali-activated concrete is limited. Hence, it is valuable to investigate the preparation of waste marble powder-slag-based alkali-activated concrete (WSAAC).

Previous research by the research group [8] has shown that waste marble powder can be used as a precursor to prepare alkali-activated concrete, and the strength of

WSAAC meets the requirements for general engineering applications. Zhang et al. [9] found that the fracture performance of alkali-activated sea coral aggregate improves with increasing alkali content. Ding et al. [10] found that increasing alkali concentration and alkali activator modulus improves the fracture performance of geopolymer concrete made with slag/fly ash. Limited research has been conducted on the fracture performance of WSAAC, making it necessary to study the fracture performance of WSAAC as an important parameter for engineering applications.

This paper aims to investigate the influence of alkali activator modulus ( $M_s$ ),  $Na_2O$  content, and slag content (SG) on the fracture properties of WSAAC. By conducting a three-point bending test, the fracture parameters of WSAAC were obtained, including  $P-CMOD$  curve,  $P-\delta$  curve, fracture toughness and fracture energy. At the same time, DIC technology was used to obtain the whole strain and displacement of WSAAC during the fracture test, which provided a reliable basis for the crack propagation path.

## 2 Experimental Design

The waste marble powder (WMP) used in this experiment is sourced from a stone processing factory in Guangxi. Its chemical composition was determined through X-ray fluorescence analysis and the results are presented in Table 1. The slag is obtained from a steel plant in Guangxi and is classified as S95-grade slag. Its chemical composition is also presented in Table 1. The fine aggregate utilized in this study is locally sourced river sand, which has a fineness modulus of 2.4, the coarse aggregate crushed limestone stones sourced locally, with a continuous grading of 5-20mm. The w/b ratio of WSAAC is 0.37, sand ratio is 0.3. The basic mix proportions are presented in Table 2.

**Table 1.** Chemical composition of waste marble powder and slag.

Name	Chemical Composition (Mass Percentage/%)						
	CaO	SiO <sub>2</sub>	Al <sub>2</sub> O <sub>3</sub>	TiO <sub>2</sub>	Fe <sub>2</sub> O <sub>3</sub>	Other	Ignition loss
WMP	54.09	1.07	1.14	0.04	0.39	0.74	42.48
SG	57.70	25.55	12.07	2.68	0.49	0.59	0.72

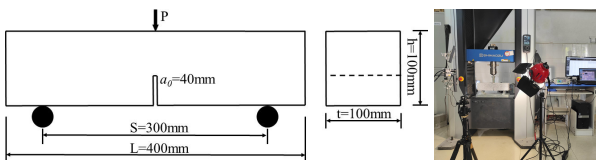


**Fig. 1.** Schematic diagram of test specimen

Three-point bending beam specimens are employed to study the fracture properties of WSAAC, as shown in Fig. 1. The loading process of the experiment is controlled by displacement, with a loading rate of 0.1mm/min.

**Table 2.** Mix proportions and fracture parameters of WSAAC.

Group	Ms	Na <sub>2</sub> O	SG	$CMOD_c$	$P_{ini}$	$P_{max}$	$a_c$	$K_{Ic}^{ini}$	$K_{Ic}^{un}$	$G_F$
		%	%	10 <sup>-3</sup> mm	kN	kN	mm	MPa·m <sup>1/2</sup>	MPa·m <sup>1/2</sup>	N/m
Ms1.0	1.0	5	35	38.3	1.37	2.06	54.4	0.32	2.36	106.5
Ms1.2	1.2	5	35	56.4	1.57	2.22	55.4	0.36	2.59	116.9
Ms1.4	1.4	5	35	41.5	1.41	2.09	54.5	0.33	2.39	147.7
Ms1.6	1.6	5	35	36.5	1.23	1.84	53.1	0.30	2.05	125.9
N3	1.4	3	35	47.4	1.34	1.96	54.4	0.32	2.26	124.2
N5	1.4	5	35	41.5	1.41	2.09	54.6	0.33	2.39	147.7
N7	1.4	7	35	44.7	1.43	2.18	54.7	0.34	2.50	163.9
SG20	1.4	5	20	53.6	0.64	0.87	46.5	0.19	0.93	84.8
SG25	1.4	5	25	41.6	0.86	1.16	48.1	0.23	1.21	106.8
SG30	1.4	5	30	50.3	1.29	1.72	52.9	0.31	1.93	138.1
SG35	1.4	5	35	41.5	1.41	2.09	54.5	0.33	2.39	147.7
SG40	1.4	5	40	46.7	2.29	3.16	63.6	0.50	4.85	177.5

Note: Ms1.0 indicates a modulus of 1.0 for alkali activator, N3 indicates a sodium oxide content of 3%, and SG20 indicates a slag content of 20%.

### 3 Experimental Results and Discussion

#### 3.1 Visualization of the Fracture Process

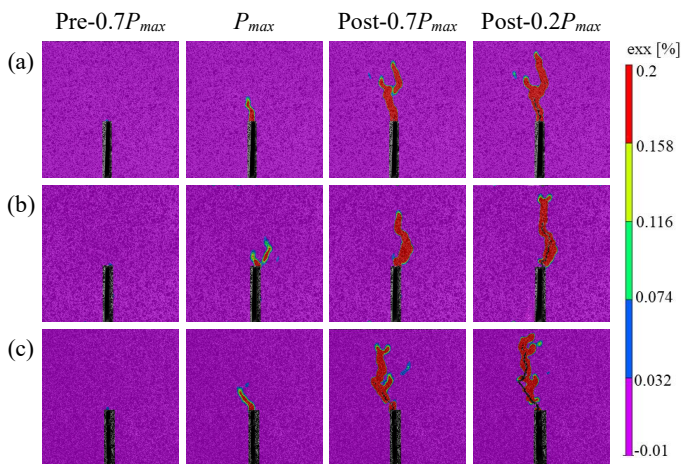


**Fig. 2.** Strain distribution maps at different loads: (a) Ms1.0, (b) N3, (c) SG20.

Fig. 2 Strain contour map shows the gradual development of strain at the pre-crack tip with increasing load throughout the entire experimental process. At 70% of the  $P_{max}$ , minimal strain is observed at the pre-crack tip, with no significant presence of cracks.

At  $P_{max}$ , significant lateral strain and stress concentration are observed at the tip of the prefabricated crack, indicating crack initiation. After  $P_{max}$ , lateral strain at the crack tip continues to increase, leading to upward crack propagation. At 20% after reaching  $P_{max}$ , the crack gradually enlarges, indicating specimen failure. Fig. 2 demonstrates that the crack propagation paths of Ms1.0, N3, and SG20 specimens exhibit a single bending trajectory, determined by the direction of principal stress after stress concentration. Cracks may encounter coarse aggregates during propagation, leading to bending development toward weaker areas.

### 3.2 P-CMOD curve and P- $\delta$ curve

Fig. 3 presents the  $P$ -CMOD and  $P$ - $\delta$  curves of all specimens, and it can be observed that the shapes of all curves are similar. The curves can be roughly categorized into three parts: linear elastic growth, crack propagation, and fracture failure. During the initial loading phase, the concrete specimens do not exhibit visible cracks and are in the linear elastic phase until the load reaches the cracking threshold. During the crack propagation stage, micro-cracks are generated and gradually enlarged at the pre-existing crack due to stress concentration. The  $P$ -CMOD curve transitions from a linear stage to a nonlinear stage as the crack expands. Crack initiation, the weak interfaces within the concrete serve as the primary path for crack propagation. As the maximum load is reached, the specimen's load-bearing capacity decreases, accompanied by a significant increase in crack opening displacement. This indicates that the specimen has entered the fracture failure stage. From Fig. 3, it can be observed that as the Ms increases, The peak load of the curve exhibits an initial upward trend followed by a subsequent decline. Additionally, with an in-crease in the  $Na_2O$  content and slag content, the corresponding peak load of the curve gradually increases.

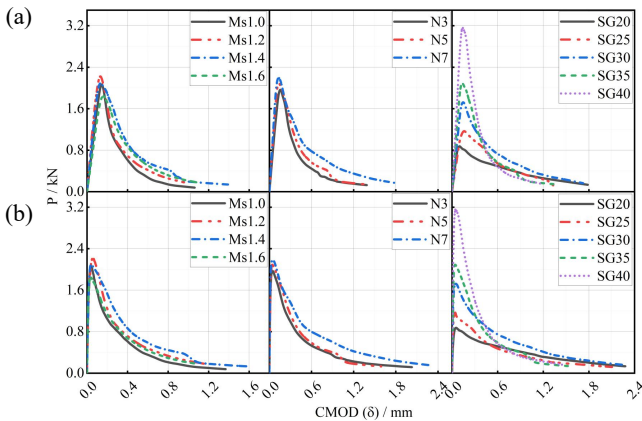


Fig. 3. The influence of different parameters on the curve: (a)  $P$ - $\delta$  curve, (b)  $P$ -CMOD curve.

### 3.3 Fracture Parameters

**Initial Fracture Toughness.** This study employs the double- $K$  fracture criterion proposed by Xu et al. [11] to determine the fracture toughness of WSAAC. The calculation formula for initial fracture toughness is as follows:

$$K_{Ic}^{ini} = \frac{1.5(P_{ini} + \frac{mg}{2} \times 10^{-2}) \times 10^{-3}}{th^2} \times S \times a_0^{1/2} \times f(a) \quad (1)$$

In the equation:  $K_{Ic}^{ini}$  represents the initial fracture toughness ( $\text{MPa}\cdot\text{m}^{1/2}$ );  $P_{ini}$  is the initiation load (kN);  $m$  is the mass between the specimen supports, converted based on  $S/L$ ;  $g$  is the gravitational acceleration, assumed to be  $9.81 \text{ m/s}^2$ .

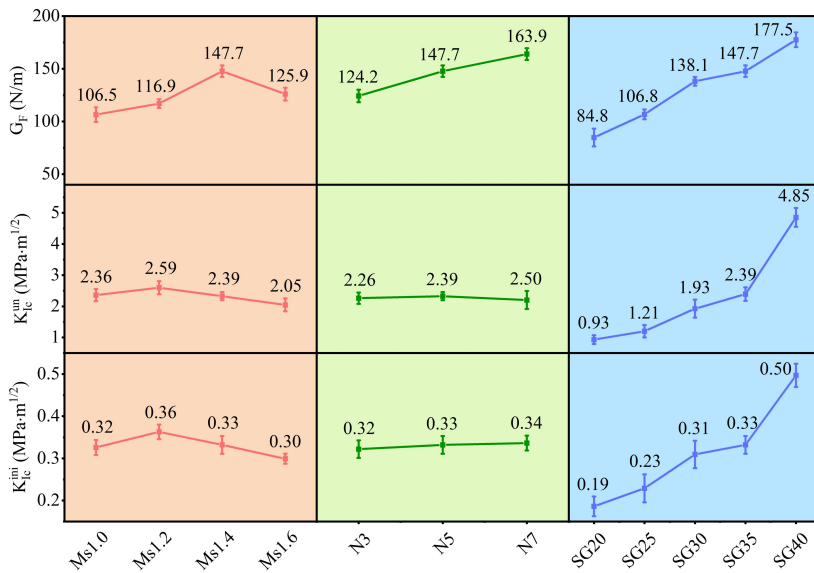


**Fig. 4.** Initial fracture toughness, unstable fracture toughness, and fracture energy for different variables.

The obtained values of  $K_{Ic}^{ini}$  for the specimens are shown in Table 2. As shown in Fig. 4, with the increase of Ms, the  $K_{Ic}^{ini}$  exhibits an initial increasing trend followed by a subsequent decrease. When increasing from Ms1.0 to Ms1.2, the  $K_{Ic}^{ini}$  increases from  $0.32 \text{ MPa}\cdot\text{m}^{1/2}$  to  $0.36 \text{ MPa}\cdot\text{m}^{1/2}$ , with an increase of 12.5%. However, when increased to Ms1.6, the  $K_{Ic}^{ini}$  decreases to  $0.30 \text{ MPa}\cdot\text{m}^{1/2}$ , with a decrease of 6.25%. With the increase of  $\text{Na}_2\text{O}$  content, the  $K_{Ic}^{ini}$  gradually increases. When increasing from N3 to N7, the  $K_{Ic}^{ini}$  increases from  $0.32 \text{ MPa}\cdot\text{m}^{1/2}$  to  $0.34 \text{ MPa}\cdot\text{m}^{1/2}$ , with an increase of 6.25%. Similarly, with the increase of slag content, the  $K_{Ic}^{ini}$  gradually increases. When increasing from 20% to 40% slag content, the  $K_{Ic}^{ini}$  increases from  $0.19 \text{ MPa}\cdot\text{m}^{1/2}$  to  $0.50 \text{ MPa}\cdot\text{m}^{1/2}$ , with an increase of 163.16%.

**Unstable Fracture Toughness.** Based on the double- $K$  fracture criterion [11], the calculation formula for unstable fracture toughness is as follows:

$$K_{Ic}^{un} = \frac{1.5(P_{max} + \frac{mg}{2} \times 10^{-2}) \times 10^{-3}}{th^2} \times S \times a_c^{1/2} \times f(a) \quad (2)$$

In the equation:  $K_{Ic}^{un}$  represents the unstable fracture toughness ( $\text{MPa}\cdot\text{m}^{1/2}$ );  $a_c$  is the effective crack length (m).

The calculated results of  $K_{Ic}^{un}$  for the specimens are shown in Table 2. As shown in Fig. 4, with the increase of Ms, the  $K_{Ic}^{un}$  exhibits an initial increase followed by a subsequent decrease. When increasing from Ms1.0 to Ms1.2, the  $K_{Ic}^{un}$  increases from  $2.36 \text{ MPa}\cdot\text{m}^{1/2}$  to  $2.59 \text{ MPa}\cdot\text{m}^{1/2}$ , with an increase of 9.75%. However, when increased to Ms1.6, the  $K_{Ic}^{un}$  decreases to  $2.05 \text{ MPa}\cdot\text{m}^{1/2}$ , with a decrease of 13.14%. With the increase of  $\text{Na}_2\text{O}$  content, the  $K_{Ic}^{un}$  gradually increases. When increasing from N3 to N7, the  $K_{Ic}^{un}$  increases from  $2.26 \text{ MPa}\cdot\text{m}^{1/2}$  to  $2.50 \text{ MPa}\cdot\text{m}^{1/2}$ , with an increase of 10.62%. Similarly, as the slag content increases, the  $K_{Ic}^{un}$  gradually increases. When increasing from SG20 to SG40, the  $K_{Ic}^{un}$  increases from  $0.93 \text{ MPa}\cdot\text{m}^{1/2}$  to  $4.85 \text{ MPa}\cdot\text{m}^{1/2}$ , with an increase of 421.51%.

**Fracture Energy.** According to the recommendations of RILEM TC-50FMC [12], the calculation formula for fracture energy is as follows:

$$G_F = \frac{W_0 + W_1}{A_{lig}}, \quad W_1 = mg\delta_{max} \quad (3)$$

Where  $G_F$  represents the fracture energy ( $\text{N/m}$ );  $W_0$  represents the area under the  $P$ - $\delta$  curve obtained from the test ( $\text{N/m}$ );  $W_1$  refers to the work done by the weight of the specimen and the test machine fixtures ( $\text{N/m}$ );  $\delta_{max}$  denotes the maximum deflection at the mid-span of the specimen (m);  $A_{lig}$  represents the area of the fracture ligament of the specimen, in square meters ( $\text{m}^2$ ).

Table 2 displays the calculated  $G_F$  values for the specimens. As shown in Fig. 4, with the increase of Ms, the  $G_F$  exhibits an initial increasing trend followed by a subsequent decrease. When increasing from Ms1.0 to Ms1.4, the  $G_F$  increases from  $106.5 \text{ N/m}$  to  $147.7 \text{ N/m}$ , with an increase of 38.69%. However, when increased to Ms1.6, the  $G_F$  is  $125.9 \text{ N/m}$ , with an increase of 18.22%. This is because alkali activators with lower Ms have a stronger alkaline property, which accelerates the early hydration of precursors but fails to fully react in later stages. Alkali activators with higher Ms produce weaker cementitious products during the reaction, resulting in a decrease in  $G_F$ . With the increase of  $\text{Na}_2\text{O}$  content, the  $G_F$  gradually increases. When increasing from N3 to N7, the  $G_F$  increases from  $124.2 \text{ N/m}$  to  $163.9 \text{ N/m}$ , with an increase of 31.96%. This is due to the high concentration of alkali, which promotes hydration of precursors and generates more hydration products. Similarly, with the increase of slag content, the  $G_F$  gradually increases. When increasing from 20% to 40% slag content, the  $G_F$  increases from  $84.8 \text{ N/m}$  to  $177.5 \text{ N/m}$ , with an increase of 109.71%. This is because the increased slag content leads to more hydration products and a denser internal structure.

## 4 Conclusions

This study conducts three-point bending tests on WSAAC with different alkali activator modulus, Na<sub>2</sub>O content, and slag content. It explores the fracture parameters and crack propagation process of WSAAC and analyzes the full-field strain using the DIC technique. Based on the experimental findings and analysis of parameters, the following main conclusions can be inferred:

- (1) With the increase of Ms, the WSAAC  $K_{Ic}^{ini}$  demonstrates an initial upward trend followed by a subsequent decline, with the highest  $K_{Ic}^{ini}$  observed for Ms1.2. With the increase of Na<sub>2</sub>O and slag content,  $K_{Ic}^{ini}$  gradually increases, with the highest  $K_{Ic}^{ini}$  observed for N7 and SG40.
- (2) With the increase of Ms,  $K_{Ic}^{un}$  displays an initial rise followed by a subsequent decline, with the highest  $K_{Ic}^{un}$  observed for Ms1.2. With the increase of Na<sub>2</sub>O and slag content,  $K_{Ic}^{un}$  gradually increases, with the highest  $K_{Ic}^{un}$  observed for N7 and SG40.
- (3) As Ms increases,  $G_F$  shows an initial upward trend followed by a subsequent downward trend, the highest  $G_F$  value is observed at Ms 1.4. With an increase in the Na<sub>2</sub>O and SG content,  $G_F$  gradually increases, the highest  $G_F$  values are observed for N7 and SG40.
- (4) The use of DIC technique allows for the comprehensive visualization of crack propagation in WSAAC, providing valuable insights into the crack growth process and morphology. It is essential in determining the fracture parameters of WSAAC.

## Acknowledgement

This study was funded by the Guangxi Science and Technology Base and Special Fund for Talents Program (Grant No. GuikeAD22035999), Guangxi Science and Technology Major Project (Grant No. GuikeAA22068073-3), the National Natural Science Foundation of China (Grant Nos. 52108201 and U22A20244), the Natural Science Foundation of Guangxi (Grant No. 2021GXNSFBA220049), the Guangxi Key Laboratory of Green Building Materials and Construction Industrialization (Grant No. 22-J-21-9).

## References

1. Turner, L.K., Collins, F.G.: Carbon dioxide equivalent (CO<sub>2</sub>-e) emissions: A comparison between geopolymer and OPC cement concrete. *Construction and building materials* **43**, 125-130 (2013)
2. Wongpaun, A., Tangchirapat, W., Suwan, T., et al.: Factors affecting compressive strength and expansion due to alkali-silica reaction of fly ash-based alkaline activated mortar. *Case Studies in Construction Materials* **19**, e02595 (2023)
3. Zhang, Z., Jia, Y., Liu, J.: Influence of Different Parameters on the Performance of Alkali-Activated Slag/Fly Ash Composite System. *Materials* **15**(8), 2714 (2022)

4. Albitar, M., Ali, M.S.M., Visintin, P., et al.: Durability evaluation of geopolymer and conventional concretes. *Construction and Building Materials* **136**, 374-385 (2017)
5. Essam, A., Mostafa, S.A., Khan, M., et al.: Modified particle packing approach for optimizing waste marble powder as a cement substitute in high-performance concrete. *Construction and building materials* **409**, 133845 (2023)
6. Batalha, Vieira, L., Francioso, V., Bueno, Mariani, B., et al.: Valorization of Marble Waste Powder as a Replacement for Limestone in Clinker Production: Technical, Environmental and Economic Evaluation. *Sustainability (Basel, Switzerland)* **15**(18), 13902 (2023)
7. Li, L.G., Huang, Z.H., Tan, Y.P., et al.: Use of marble dust as paste replacement for recycling waste and improving durability and dimensional stability of mortar. *Construction and Building Materials* **166**, 423-432 (2018)
8. Liu, B., Geng, S., Ye, J., et al.: A preliminary study on waste marble powder-based alkali-activated binders. *Construction and Building Materials* **378**, 131094 (2023)
9. Zhang, B., Zhu, H., Lu, F.: Fracture properties of slag-based alkali-activated seawater coral aggregate concrete. *Theoretical and applied fracture mechanics* **115**, 103071 (2021)
10. Ding, Y., Shi, C., Li, N.: Fracture properties of slag/fly ash-based geopolymer concrete cured in ambient temperature. *Construction and Building Materials* **190**, 787-795 (2018)
11. Xu, S., Reinhardt, H.W.: Determination of double- $K$  criterion for crack propagation in quasi-brittle fracture, part I: Experimental investigation of crack propagation. *International Journal of Fracture* **98**(2), 111-149 (1999)
12. RILEM.: Determination of the fracture energy of mortar and concrete by means of three-point bend tests on notched beams. *Materials and Structures* **18**(4), 287-290 (1985)

**Open Access** This chapter is licensed under the terms of the Creative Commons Attribution-NonCommercial 4.0 International License (<http://creativecommons.org/licenses/by-nc/4.0/>), which permits any noncommercial use, sharing, adaptation, distribution and reproduction in any medium or format, as long as you give appropriate credit to the original author(s) and the source, provide a link to the Creative Commons license and indicate if changes were made.

The images or other third party material in this chapter are included in the chapter's Creative Commons license, unless indicated otherwise in a credit line to the material. If material is not included in the chapter's Creative Commons license and your intended use is not permitted by statutory regulation or exceeds the permitted use, you will need to obtain permission directly from the copyright holder.

